

# Lawrence Berkeley National Laboratory

## Lawrence Berkeley National Laboratory

### Title

Time-resolved measurements of desorbed gas during 1-MeV K<sup>+</sup> pulsed beam deposition in a stainless steel target

### Permalink

<https://escholarship.org/uc/item/6sv0r8zq>

### Authors

Bieniosek, F.M.  
Prost, L.R.  
Seidl, P.A.  
et al.

### Publication Date

2008-05-15

**Time-resolved measurements of desorbed gas during 1-MeV  $K^+$  pulsed beam deposition in a stainless steel target**

F.M. Bieniosek\*, L.R. Prost†, and P.A. Seidl

*Lawrence Berkeley National Laboratory, Heavy Ion Fusion Science Virtual National Laboratory, 1 Cyclotron Road, Berkeley, California 94720 USA*

A.W. Molvik and M. Kireeff Covo

*Lawrence Livermore National Laboratory, Heavy Ion Fusion Science Virtual National Laboratory, Livermore, California 94550 USA*

*Abstract*

Measurements were made of the density, species and velocity of the desorbed gas cloud on intense  $K^+$  beam bombardment of a stainless steel target. RGA measurements indicate that the gas cloud consists of predominantly  $H_2$ . Energy analyzer measurements of doubly-ionized beam ions show that the ratio of hydrogen gas production to beam density was approximately 3000 at normal incidence. Optical measurements of the evolution of the gas cloud during the beam pulse show a distribution with an average expansion velocity of about  $0.5 \text{ mm}/\mu\text{s}$ . Comparison is made with a simple model of the gas cloud behavior.

PACS 52.59.-f, 52.58.Hm, 52.70.-m, 52.70.Kz

\*Electronic address: [fmbieniosek@lbl.gov](mailto:fmbieniosek@lbl.gov)

†Current address: Fermi National Accelerator Laboratory, Batavia, Illinois 60510 USA

## I. INTRODUCTION

Beams of heavy ions release large amounts of neutral gas when they strike the vacuum wall. This effect [1], and the related problem of electron cloud [2], can have a serious deleterious effect by causing local pressure rise that limits the performance of particle accelerators. Based on measurements of pressure rise, the desorption coefficients have previously been determined to be about 10,000 for 1 MeV  $K^+$  ions at near grazing incidence on stainless steel walls [3].

We develop here two new independent techniques of estimating the gas production. The first technique is based on measurement of the flux of  $K^{++}$  ions produced by ionization of incident  $K^+$  beam ions  $K^+ \rightarrow K^{++}$  in the gas cloud.

In the second technique we observe the optical emission of the gas cloud excited by the incoming ion beam. This technique follows the one-dimensional (1-D) formation and evolution of the gas cloud produced when an intense heavy ion beam strikes the vacuum wall at normal incidence. We compare these observations with the predictions of a simple 1-D model for expansion of the cloud.

## II. APPARATUS

The HCX (High Current Experiment) [4] at Lawrence Berkeley National Laboratory is designed to explore the physics of intense heavy-ion beam transport in the context of developing a driver for heavy-ion inertial fusion energy production [5]. Typical  $K^+$  beam current is 0.18 A at an energy of 1 MeV. The energy analyzer measurements were performed downstream of the electrostatic quadrupole injector, matching section and electrostatic transport section as described in [4]. The optical measurements were performed between the second and third magnetic quadrupoles of the magnetic transport section as depicted in Fig. 1, which was installed immediately downstream of the electrostatic transport section after the energy analyzer measurements were completed.

As the ion beam strikes a solid target, it desorbs gas trapped on or near the surface of the wall. The  $K^{++}$  ions are generated by ionization of the incident  $K^+$  ion beam by the gas cloud created at the entrance slit of the analyzer or at the hole plate upstream of the analyzer. The intensity of the  $K^{++}$  ion signal provides an estimate of the rate of production of the gas cloud. Thereby the rate and number of gas atoms instantaneously released per incident beam ion on the wall under the conditions of this experiment is determined.

For the optical measurements, a stainless steel (type 304) target was mounted on a movable paddle and inserted into the path of the ion beam. No special cleaning techniques were used on the target. The vacuum system consisted of oil-free turbo and cryo pumps.

The optical images were taken by a high speed image-intensified CCD camera (Princeton Instruments PI-MAX) imaging the gas cloud at a right angle to the beam. The camera is capable of taking a single gated image per beam pulse.

A Stanford Research System Residual Gas Analyzer, RGA-300, with a fast direct analog output (ion counting output), was installed at a port within about 40 cm of the target. It measured the local gas density increase immediately after the beam pulse.

The electrostatic energy analyzer (EEA) used in these experiments was a  $90^\circ$  cylindrical sector field analyzer with first-order focus [6]. The EEA has a radius of curvature of 45.72 cm, a separation between plates of 2.54 cm (Fig. 2). The deflection plate voltages to provide the  $90^\circ$  sector bend field for a 970-keV ion beam are  $\pm 54$  kV for  $K^+$  and  $\pm 27$  kV for  $K^{++}$ . A drift region extends before and after the sector field to provide the first-order focus of the entrance slit at the detector plane. The entrance slit provides collimation for the measurements; its dimensions are 0.05 cm x 6.64 cm in a stainless steel foil; the slit-cup detector has an entrance slit width of 0.010 cm.

The EEA was mounted at the end of the diagnostic tank such that the entrance slit was 1.5 m downstream of the last HCX quadrupole. A slit-cup detector was located at the image plane of the analyzer with the 0.1-mm slit aligned on the center path between the

deflecting electrodes. In addition to its utility as an energy analyzer, the EEA can distinguish a weak signal of doubly-ionized  $K^{++}$  ions from the intense incident  $K^+$  beam. This is done by operating the analyzer at exactly half of the voltage appropriate for  $K^+$  beam ions. A 23% transparency hole plate (304 SS, 76  $\mu\text{m}$  hole diameter with 152  $\mu\text{m}$  separation on a hexagonal pattern), [Buckbee-Mears BE 0201 (now Internet, Inc.)] was installed on a movable drive 69 cm upstream of the analyzer entrance slit to provide higher charge-state ions for the measurement of gas production.

Emission profiles are a measure of the rate of decay of excited states of the gas molecules. During the beam pulse, the gas molecules are continuously excited by the passage of the intense ion beam. After the end of the beam pulse, some residual radiation continues to be observed with a decay time of several  $\mu\text{s}$ . The spectrum of this residual radiation is not the same as that of the emission during the beam pulse. The residual radiation may be due to the decay of relatively long-lived metastable excited states of the gas molecules.

### III. RESULTS

#### A. Composition of desorbed gas

The base pressure in the vacuum system was approximately  $1 \times 10^{-7}$  Torr, consisting of primarily  $\text{H}_2\text{O}$ ,  $\text{N}_2$ , and  $\text{O}_2$  gas.

RGA signals were measured for a number of atomic masses with time resolution of about 40 ms. The instantaneous time response of the signals showed a rapid increase in signal at the time of beam firing, with a subsequent exponential decay rate of 100-250 ms, depending on the atomic number being monitored. A trend with atomic number was observed; the signal for small atomic numbers decayed faster than for large atomic numbers (up to 56 AMU).

Fig. 3 summarizes the zero-time intercepts of the RGA signals. These are extrapolated to time  $t = 0$  from the exponential decay of the RGA signal for each ion mass. They have been corrected for the relative sensitivity of the RGA for the known gas species. Each data point in the figure represents the zero-time intercept of the signal from a single beam pulse at the given mass number. The results indicate that most (85%) of the gas released is hydrogen (1 or 2 AMU). Approximately 7% is mass 28 (CO or  $\text{N}_2$ ), with all other mass species <2%. This species mix characteristic of the instantaneous wall desorption differs substantially from the baseline residual gas.

#### B. Optical measurement of the gas expansion

Optical measurements of the gas cloud were performed viewing at right angle to the beam at a plate inserted in the path of the HCX beam (Fig. 1). The beam ions interact with the gas cloud to generate light as the beam excites states in the atoms and molecules in the gas cloud. By varying the time gating of the camera, it is possible to construct a time history of the gas cloud during the beam pulse.

A series of images taken with the PI-MAX camera at  $0.5 \mu\text{s}$  intervals shows growth and decay of the gas cloud as a function of time (Fig. 4).

A line integral of the images was constructed to create what is effectively a streak camera image. These images were constructed by integrating each image along a vertical line to generate a curve of total light intensity as a function of position from the target. Assembling the curves produces Fig. 5, which shows a false-color image of the optical signal as a function of position and time. The image shows the expansion of the cloud, with an edge expansion velocity of roughly  $1.5 \text{ mm}/\mu\text{s}$ . The gas cloud was imaged in three colors – blue, green and red filters (Wratten numbers 29, 11, and 47B). The three streak images, summarized in Fig. 6, show much the same expansion velocity in the three

colors, with some differences, primarily in the residual optical emission after the end of the beam pulse. The gas cloud emission was roughly uniform across the optical spectrum during the beam pulse, and it fluoresced predominantly in the green afterwards. The overall mean gas velocity was  $0.5 \text{ mm}/\mu\text{s}$ , consistent across the optical spectrum. This corresponds to a fixed mean directed velocity of a Maxwellian distribution  $\bar{v}/4$ , and is consistent with a gas cloud dominated by neutrals of a single mass or similar masses. The value for  $\bar{v}/4$

$$\frac{\bar{v}}{4} = \sqrt{\frac{kT}{2\pi m}}$$

at a temperature of  $20 \text{ }^\circ\text{C}$  is  $440 \text{ m/s}$  for molecular hydrogen  $\text{H}_2$ , and  $623 \text{ m/s}$  for atomic hydrogen  $\text{H}$ . The measured velocity corresponds to a distribution of  $\text{H}_2$  molecules near room temperature; the possibility that the gas cloud is emitted in the form of predominantly atomic  $\text{H}$  is ruled out because the expansion velocity is slower than the thermal expansion velocity for an atomic hydrogen cloud. In addition the optical emission spectrum imaged by an optical spectrometer lacked strong line structure, such as the Balmer lines of atomic hydrogen (H-alpha, H-beta, etc.). This result is consistent with the band structure of the spectrum of molecular  $\text{H}_2$  [7].

Line-integrated total light profiles show the growth, expansion, and decay of the gas cloud [Fig. 7]; the total imaged light increased roughly linearly during the beam pulse, then decayed slowly afterwards.

### C. Energy analyzer measurements

The analyzer entrance aperture was  $130 \text{ cm}$  downstream of the exit of the HCX magnetic transport section. In this field-free drift region the ion beam was allowed to expand to a beam size approximately  $3 \text{ cm} \times 10 \text{ cm}$  at the analyzer location, as estimated by a beam envelope code.

As the beam strikes the steel wall surrounding the holes in the hole plate or the analyzer entrance slit, gas is released from the wall. The gas forms a cloud that expands at a rate characterized by its directed velocity. For  $\text{H}_2$ , the directed velocity is  $440 \text{ m/s}$  for a gas temperature  $T = 20 \text{ }^\circ\text{C}$  as discussed above. This velocity is sufficient to expand uniformly into the holes in the hole plate and into the  $0.5\text{-mm}$  analyzer entrance slit on time scale much less than the beam pulse length,  $\tau \ll 4 \mu\text{s}$ .

Measurements discussed here were performed with the hole plate inserted in the path of the beam, upstream of the EEA. It was inserted for three reasons: 1. The hole plate can be biased to distinguish production of  $\text{K}^{++}$  at the hole plate from production at the analyzer entrance slit; 2. The hole plate reduces the  $\text{K}^{++}$  beam intensity in the vicinity to minimize beam loading on the analyzer plates; 3. The hole plate provides an independent

$K^{++}$  signal at greatly different source density to compare with the  $K^{++}$  signal from the analyzer entrance slit. In this way it is possible to estimate the effect of charge exchange, as discussed below.

Measurements of the beam current transported through the analyzer were performed by adjusting the analyzer deflection voltage in 40 V increments for  $K^+$  and 20 V increments for  $K^{++}$ , to map out the beam energy distribution as a function of time on a pulse-by-pulse basis. These increments correspond to a transverse variation of the beam at the detector location of 0.034 cm per increment.

Fig. 8 shows the transported beam current taken from a scan of the  $K^+$  beam. The raw signals from a series of measurements taken with a fixed increment in analyzer voltage were summed and scaled by the following factors to yield the total beam current transported through the analyzer,  $i_+$ .

$$i_+ = \frac{s}{wR(\delta + 1)}V$$

where  $V$  is the detector signal in volts,  $w$  is the detector slit width (0.01 cm),  $R$  is the viewing resistor (50  $\Omega$ ),  $\delta$  is the secondary electron emission coefficient for the ion beam ( $\approx 20$ ), and  $s$  is the step increment of the measurements (0.034 cm).

These measurements were taken with a negatively-biased collector behind the detector slit. The signal represents the sum of the ion beam current and the secondary electron current produced at the detector plate by the incident beam ions. The measured total  $K^+$  beam signal corresponds to a beam current of about 230  $\mu\text{A}$  transported through the analyzer.

The  $K^+$  signal intensity as a function of time and voltage is shown in Fig. 9a. The shape of the longitudinal beam energy distribution is described in detail in Ref. 4.

Similarly, an intensity plot of the  $K^{++}$  signal as a function of time and analyzer voltage is shown in Fig. 9b. It is necessary to distinguish the  $K^{++}$  ions created at the entrance slit from the  $K^{++}$  ions created at the hole plate. They can be distinguished by the different energy of the two populations. The plot clearly shows two distributions; the upper distribution corresponds to the  $K^{++}$  ions created at the hole plate, with a bias of 9.5 kV, and the lower distribution corresponds to the  $K^{++}$  ions created at the entrance slit, which is grounded.

Fig. 10 shows the sum signal taken from a scan of the  $K^{++}$  signal, again taking into account the known step size increments. It has been scaled in a manner similar to that described above for the  $K^+$  signal.

$$i_{++} = \frac{s}{wR(\delta + 2)} \frac{1}{A_g} V.$$

These measurements were also taken with a negatively-biased collector, and with an additional amplifier of gain  $A_g = 50$ . The total  $K^{++}$  particle current at the peak is  $3.5 \mu\text{A}$ . After the upper distribution from the hole plate is removed, the peak particle current from the slit is  $1.14 \mu\text{A}$ .

The ratio of the two ion currents ( $K^{++}$  from the analyzer entrance slit) / ( $K^+$  from the beam) is .005. This ratio is a direct measure of the product of the line density of the gas cloud at the entrance slit, and the ionization cross section,  $\langle nl \rangle \sigma_{12}$ . The time-integrated flux density of incident beam ions at the time of the peak  $K^{++}$  signal (the  $K^{++}$  signal was truncated in taking the data at late times) is  $n_b = \frac{1}{A_{slit}} \int i_+ dt = 1.6 \times 10^{10} \text{ cm}^{-2}$  where  $A_{slit} = 0.332 \text{ cm}^2$  is the area of the slit. Note that the integral is taken up to the time of the peak of the  $K^{++}$  signal, not the end of the  $K^+$  pulse.

The ionization cross section  $\sigma_{12}$  for a  $K^+$  beam ( $K^+ \rightarrow K^{++}$ ) on  $\text{H}_2$  has been measured up to 600 keV;  $\sigma_{12}$  at 600 keV is  $\sigma = 1.14 \times 10^{-16} \text{ cm}^2$  [8]. Since the ionization cross section dependence on energy is relatively flat in this range, we use this value for  $\sigma_{12}$  at the experimental beam energy (970 keV).

For  $\langle nl \rangle \sigma_{12} = .005$ , and  $\sigma_{12} = 1.14 \times 10^{-16} \text{ cm}^2$ , the line density of gas is  $\langle nl \rangle = 4.4 \times 10^{13} \text{ cm}^{-2}$ . The number of gas particles at the slit per incident ion beam is then simply the ratio  $\langle nl \rangle / n_b = 2740$ . The rate of  $K^{++}$  production is directly proportional to the instantaneous gas line density and the beam current; both increase linearly during the beam pulse, as seen in Fig. 10. At the end of the beam pulse the  $K^{++}$  current also drops to zero as expected.

#### IV. SOURCES OF ERROR IN THE MEASUREMENT

Depletion due to charge exchange. Charge exchange ( $K^{++} \rightarrow K^+$ ) is an exchange of a single electron between the doubly-charged  $K^{++}$  ion and a neutral gas molecule. Neglecting other possible charge-changing reactions, it involves a two-step process in which an incident  $K^+$  ion is first ionized to  $K^{++}$  in the gas cloud; then the  $K^{++}$  ion recaptures an electron from a gas molecule before leaving the gas cloud. If the rates for both reactions are small  $\langle nl \rangle \sigma \ll 1$ , then the  $K^{++}$  is created uniformly throughout the gas cloud, and the average path length traversed by a  $K^{++}$  ion is  $\langle nl \rangle / 2$ . The fraction of the  $K^{++}$  ions that undergoes charge exchange is then  $\frac{1}{2} \langle nl \rangle \sigma_{21}$ .

The charge exchange process is energetically favorable and the cross sections tend to be large. The closest available data for the measured charge-changing cross section is  $\sigma_{21} = 8 \times 10^{-16} \text{ cm}^2$  for  $K^{++}$  on  $\text{N}_2$  and  $3 \times 10^{-15} \text{ cm}^2$  at 120 keV for  $K^{++}$  on  $\text{O}_2$  [9]. In addition Betz [10] shows that the equilibrium charge fraction for a 1-MeV potassium beam in gas is approximately 1, also indicating that  $\sigma_{21}$  is large. Using the larger of the two data

points from Ref. 9, charge exchange would deplete only 2% of the  $K^{++}$  ions created at the analyzer entrance slit.

In contrast, the intensity of  $K^{++}$  ions created at the hole plate is depleted from the amount expected based simply on the beam current density. The beam envelope model indicates that the incident beam intensity and thus line density of liberated gas at that location should be about 20 times larger than at the analyzer entrance slit. The higher gas density should lead in turn to both a higher  $K^{++}$  ion flux, and a higher charge exchange fraction, estimated in the range of 40%. In the absence of charge exchange, and taking into account the transparency of the hole plate, the signal from the hole plate should be about  $20 \times 0.23 = 4.6$  times larger than the signal from the slit. In fact, the signal from the hole plate is about a factor of 4 larger early in the pulse, and a factor of 2 larger late in the pulse. The amount of observed depletion of  $K^{++}$  created at the hole plate is consistent with the expectation that the charge-changing cross section at 970 keV is comparable to that at the measured data point (120 keV). Because of the large depletion, analysis of  $K^{++}$  created at the hole plate would underestimate gas production. Thus the population of  $K^{++}$  from the hole plate is not used in the determination of gas production.

Penetration of gas through and behind the slit. The presence of the slit reduces the transient local density of the gas cloud. The density perturbation may be estimated by considering the horizontal position  $x$  of a Gaussian distribution of particles generated at each point  $x_i$  along the surface of the wall at time  $t$  after the particle distribution is generated:

$$g(x, x_i) = \exp\left(-\frac{m}{2kT} \left(\frac{x - x_i}{t}\right)^2\right)$$

where  $(x-x_i)/t = v_x(t)$  represents the x-directed velocity of the molecule. The local gas density in the vicinity of the slit at time  $t$  is the integral

$$f(x) = \int_{-\infty}^a g(x, x_i) dx_i + \int_b^{\infty} g(x, x_i) dx_i$$

where  $a$  and  $b$  represent the locations of the edges of the slit. The gas density averaged over the slit  $\bar{h}_{slit}$  at time  $t$  is

$$\bar{h}_{slit} = \frac{1}{b-a} \int_a^b f(x) dx .$$

Finally if gas production is a function of time,  $h=h(t)$ , the slit-averaged density is the convolution

$$\bar{n}_{slit}(t) = \int_0^t \bar{h}_{slit}(t-\tau)n(\tau)d\tau.$$

For a constant beam current-density pulse,  $j = \text{const.}$  for  $0 < t < t_{pulse}$ , the gas density follows the integral of the current pulse:  $n(t) = n_0 t/t_{pulse}$ , for  $t < t_{pulse}$  and  $n(t) = n_0$ , for  $t \geq t_{pulse}$ . The ratio of the calculated slit-averaged density  $\bar{n}_{slit}(t)$  to the gas density at the edge of the slit during the beam pulse for  $H_2$  gas at  $20^\circ C$  is  $\sim 0.9$ . Thus a small correction of  $1/0.9$  due to this effect should be applied to the estimate for gas production. The effective gas desorption coefficient is therefore approximately 3000.

## V. MODEL OF GAS PROFILE

We model the expansion of the gas from the wall as a 1-D expansion, i.e. the distance from the wall is less than the transverse extent of the beam at the target. Models for 1-D expansion of a desorbed gas into a vacuum are described in detail in Refs. 11 and 12. In the case of an intense release of gas, i.e. when the number of monolayers released is  $\gg 1$ , the gas dynamic equations take on a relatively simple form. Assume that the gas obeys the adiabatic law

$$n = \text{const} \cdot c^{2/(\gamma-1)}$$

where  $\gamma$  is the ratio of specific heats,  $n$  is the density, and  $c$  is the velocity of sound. The gas flow is described by the continuity and Euler equations. For time  $t < \tau$  the solution of the system of equations is given in normalized coordinates. The time  $t$  is scaled by  $\tau$ , flow velocity  $u$  by the velocity at the Knudsen layer on the surface of the target,  $u_k = \sqrt{\gamma(kT_k/m)}$ , and the distance  $x$  from the surface of the target by  $x_k = u_k \tau$  for  $c > 0$ . The constants  $T_k$  and  $n_k$  are the temperature and density of the surface layer.

$$u(x,t) = 1 + \frac{2}{\gamma+1} \frac{x}{t}$$

$$c(x,t) = 1 - \frac{\gamma-1}{\gamma+1} \frac{x}{t}$$

Therefore the density can be written as

$$n(x,t) = n_0 \left( 1 - \frac{\gamma-1}{\gamma+1} \frac{x}{t} \right)^{2/(\gamma-1)}.$$

Note that contours of constant density are straight lines on an  $x$  vs.  $t$  plot, in agreement with the measured contours of Fig. 6. The model density profiles are plotted for  $H_2$  gas ( $\gamma = 1.4$ ), together with the experimental image intensity profiles, in Fig. 11. Measured gas expansion is generally slower than predicted by the model for  $20^\circ C$ ; comparison between

the data and the model suggests a Knudsen temperature much lower than the surface temperature.

After the end of the beam pulse,  $t > \tau$ , the behavior becomes more complicated and depends on the reflection properties of the gas particles on the wall surface. Reflection of the particles leads to a wave that travels into the gas cloud beginning at  $t = \tau$  at the surface. In the low-density case of a halo scraping the walls, the evolution of gas will be similar in form but may be modeled by the rate of expansion of the gas molecules into the vacuum.

## VI. DISCUSSION

The rate of gas production is measured with excellent time resolution. The results verify that, as expected, large amounts of gas are released from the wall in the beam-wall interaction. The gas production is shown to be instantaneous and directly proportional to the incident ion beam intensity up to the intensity used in these experiments. These techniques are not sensitive to gas desorption after the beam pulse.

The yield of desorbed gas molecules is expected to vary widely with respect to wall surface conditions such as cleanliness, surface roughness, history, and type of material. Therefore the measured gas yield should be considered an approximate guide to the yield under any given set of conditions.

The yield derived here,  $\sim 3000$  adsorbed gas molecules per beam ion at normal incidence, may be compared with other measurements of gas production [13, 14]. Published measurements vary widely over a wide range. There are several possible reasons for the wide range and discrepancy, in addition to the effects of surface condition. One reason is that many measurements are typically taken at near grazing incidence, where the numbers are expected to be larger than at normal incidence. For example the gas desorption coefficient of 10,000 for similar beam conditions at grazing incidence presented in Ref. 3 extrapolates to about 3000 at normal incidence. Another reason is that time-integrated gas production monitored by a vacuum pressure gauge typically measures gas after one or several bounces off the vacuum wall, whereas the technique described here measures the instantaneous local gas production during the beam pulse.

This technique has application as an alternative to the conventional techniques for measuring heavy-ion-beam-induced adsorption of gas from the wall. The advantage is that the measurement is direct and instantaneous during the time of the beam pulse.

Further measurements that can be made include

- measuring instantaneous gas production as a function of angle of incidence by passing the beam through a pivoted slit or aperture plate
- measuring effects of wall material and condition on gas cloud species and quantity.

## ACKNOWLEDGEMENTS

The authors gratefully acknowledge the support of W. Greenway, T. Katayanagi and the LBNL technical staff. This work was performed under the auspices of the U.S Department of Energy by University of California, Lawrence Livermore and Lawrence Berkeley National Laboratories under contracts No. W-7405-Eng-48 and DE-AC03-76SF00098.

## REFERENCES

1. A.W. Molvik, H. Kollmus, E. Mahner, M. Kireeff Covo, M.C. Bellachioma, M. Bender, F.M. Bieniosek, E. Hedlund, A. Krämer, J. Kwan, O.B. Malyshev, L. Prost, P.A. Seidl, G. Westenskow, and L. Westerberg, *Phys. Rev. Lett.* 98, 064801 (2007).
2. Proceedings of the Workshop on Electron-Cloud Simulations for Proton and Positron Beams (E-CLOUD02), CERN, Geneva, 15-18 April 2002, edited by F. Ruggiero, J. Thomashausen, and F. Zimmerman (CERN, Geneva, 2002), URL: <http://wwwslap.cern.ch/collective/ecloud02/proceedings>.
3. A.W. Molvik, M. Kireeff Covo, F.M. Bieniosek, L.R. Prost, P.A. Seidl, D. Baca, A. Coorey, A. Sakumi, *Phys. Rev. Spec. Top.-AB 7*, 093202 (2004).
4. L.R. Prost, P.A. Seidl, F.M. Bieniosek, C.M. Celata, A. Faltens, D. Baca, E. Henestroza, J.W. Kwan, M. Leitner, W.L. Waldron, R. Cohen, A. Friedman, D. Grote, S.M. Lund, A.W. Molvik, E. Morse, *Phys. Rev. Spec. Top.-AB 8*, 020101 (2005)
5. B.G. Logan, F.M. Bieniosek, C.M. Celata, E. Henestroza, J.W. Kwan, E.P. Lee, M. Leitner, P.K. Roy, P.A. Seidl, S. Eylon, J.-L. Vay, W.L. Waldron, S.S. Yu, J.J. Barnard, D.A. Callahan, R.H. Cohen, A. Friedman, D.P. Grote, M. Kireeff Covo, W.R. Meier, A.W. Molvik, S.M. Lund, R.C. Davidson, P.C. Efthimion, E.P. Gilson, L.R. Grisham, I.D. Kaganovich, H. Qin, E.A. Startsev, D.V. Rose, D.R. Welch, C.L. Olson, R.A. Kishek, P. O'Shea, I. Haber and L.R. Prost, Overview of US heavy ion fusion research, *Nucl. Fusion*, 45, 131-137 (2005).
6. R. E. Warren, J. L. Powell, R. G. Herb, *RSI* 18, 559 (1947).
7. H. G. Gale, G. S. Monk, and K. O. Lee, *The Astrophysical Journal* 67 (1928) p. 89-113.
8. I. Alvarez, C. Cisneros, C.F. Barnett, and J.A. Ray, *Phys. Rev.* A13, 1728-1733 (1976).
9. H.H. Lo, W.L. Fite, *Atomic Data* 1, 305 (1970)
10. H.D. Betz, *IEEE Trans. Nucl. Science NS-18*, 1110 (1971)
11. D. Sibold and H.M. Urbassek, *Phys. Rev. A* 43, 6722-6734 (1991).
12. D. Sibold and H.M. Urbassek, *Phys. Fluids A4*, 165-177 (1991).
13. E. Mahner, J. Hansen, D. Kuechler, M. Malabaila, M. Taborelli, *Phys. Rev. Spec. Top.-AB 8*, 053291 (2005).

14. R. Behrisch, V.M. Prozesky, H. Huber, W. Assman, Nucl. Instrum. Meth. B 118, 262-267 (1996).

15.

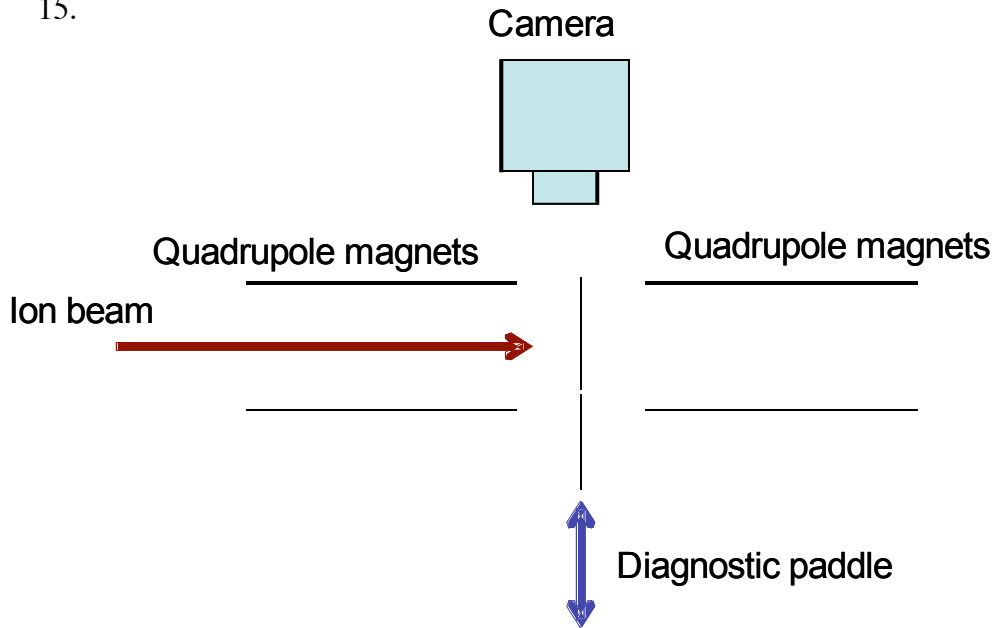


Fig. 1. Schematic of the optical measurement in the magnetic transport section of HCX. The ion beam enters from the left (red arrow) and passes through a series of 4 quadrupole magnets. The diagnostic paddle is inserted into the path of the beam between the second and third magnets. The camera views the front of the diagnostic paddle from the side.

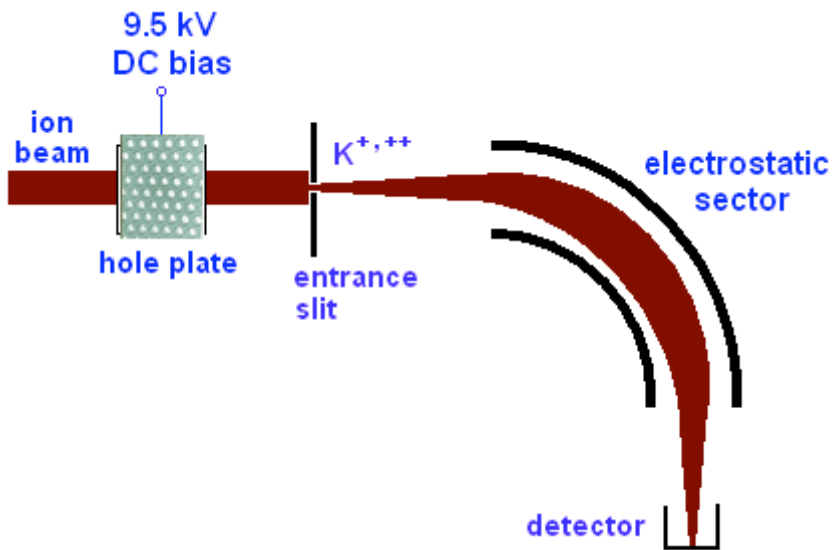


Fig. 2. Simplified schematic diagram of the electrostatic energy analyzer.

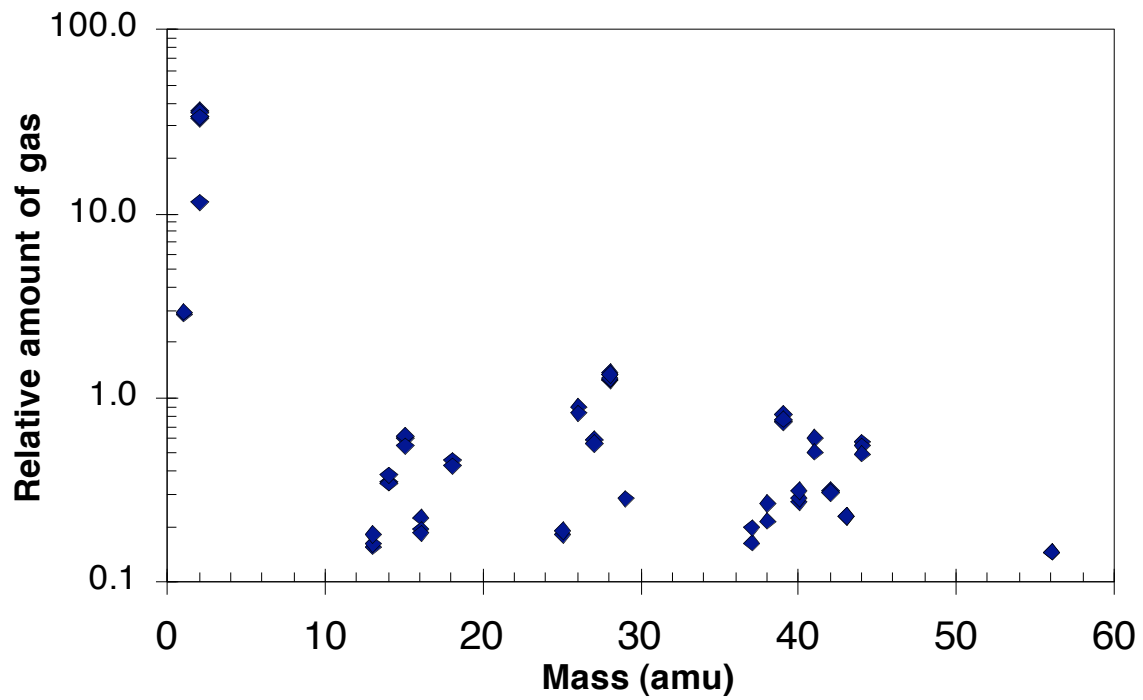


Fig. 3. Fast RGA spectrum as a function of atomic mass number AMU.

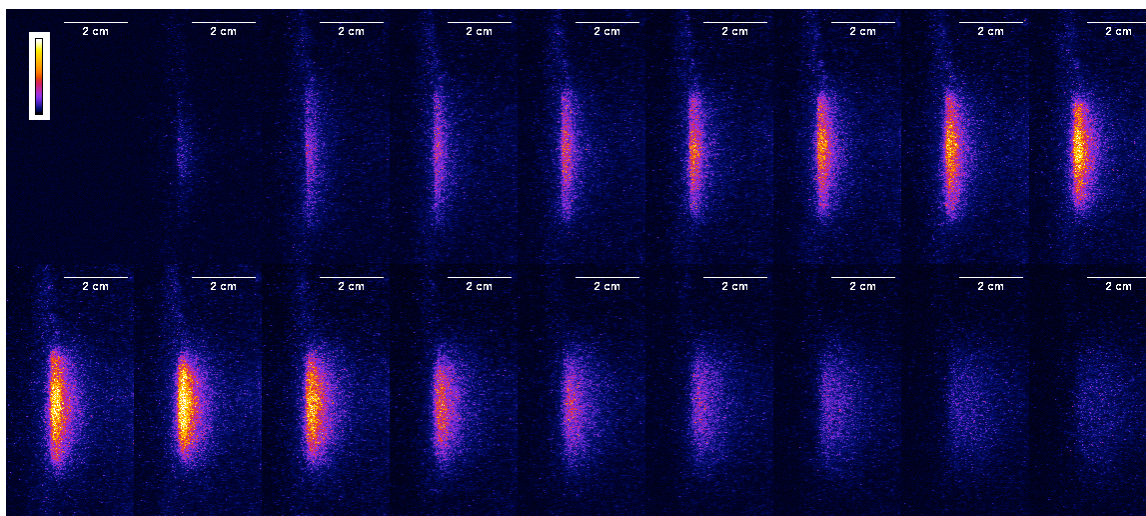


Fig. 4. Images of the gas cloud taken at 0.5 μs delay intervals.

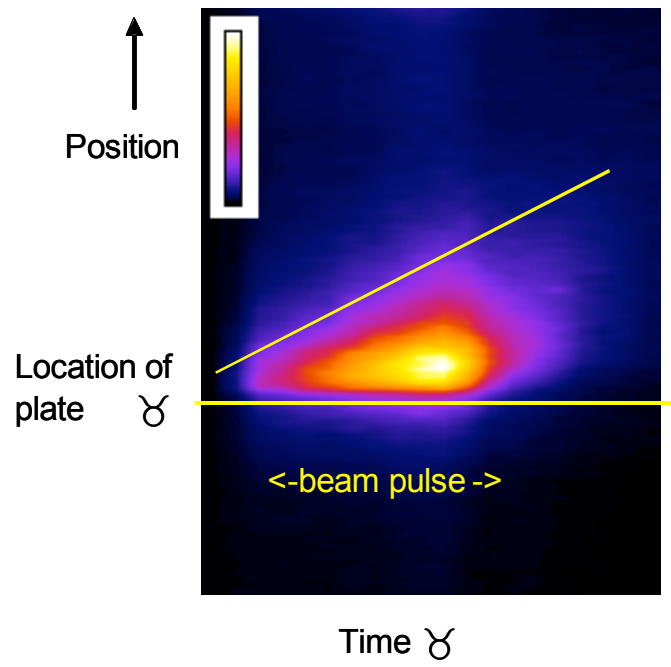


Fig. 5. Line integral of the images of Fig. 4. The sloped line indicates an expansion rate of  $1.5 \text{ mm}/\mu\text{s}$ . The beam pulse is  $4 \mu\text{s}$  long.

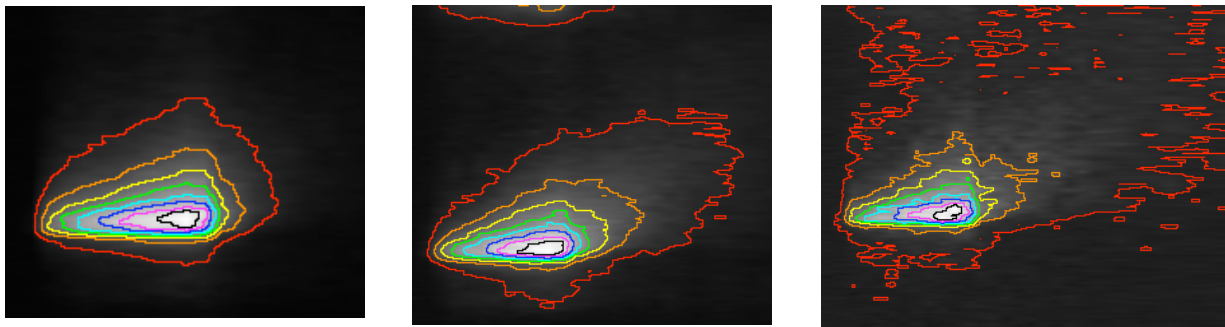


Fig. 6. Gas cloud imaged in blue, green and red. Shown are contours of constant light intensity.

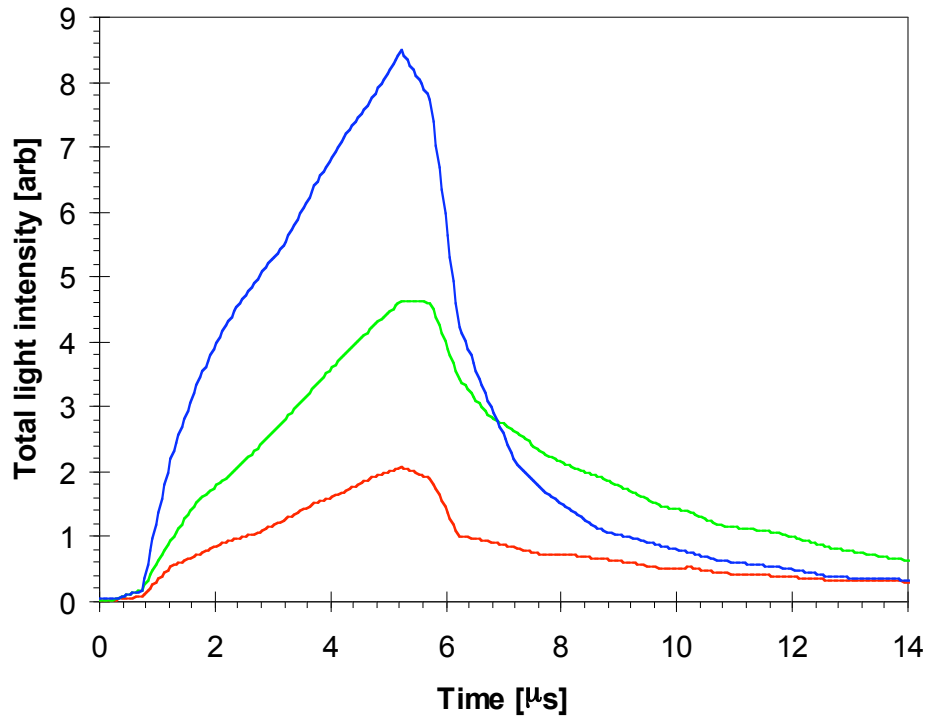


Fig. 7. Line integrated light profiles in red, green, and blue – total emission from the entire cloud. The relative intensity of the three colors is not significant – the sensitivity of the camera image intensifier peaks in the blue.

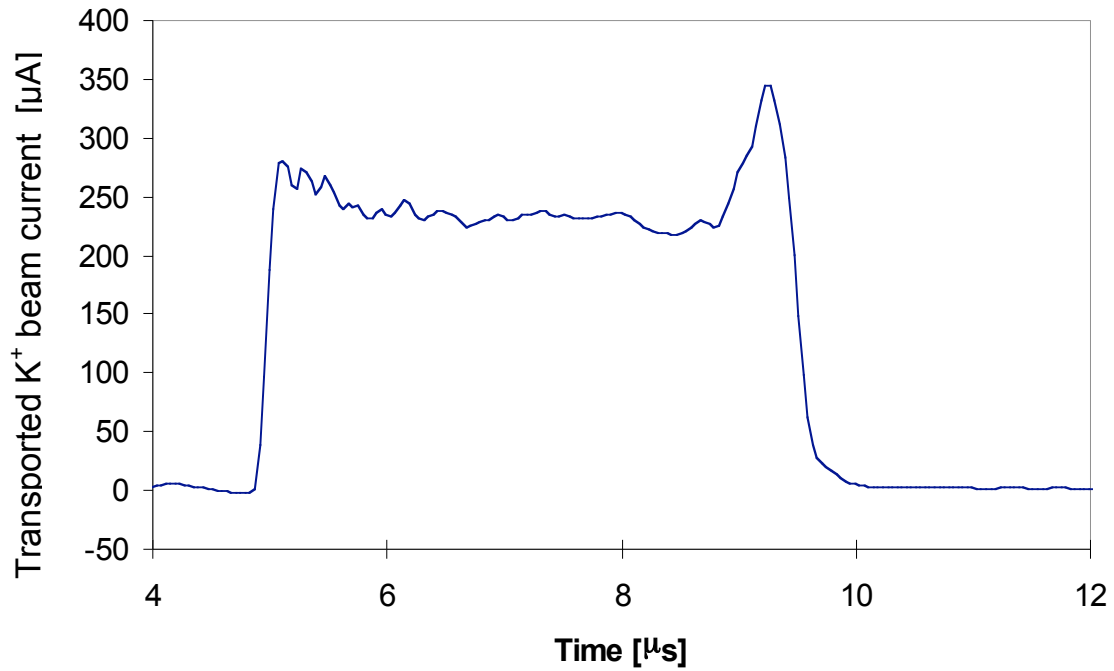


Fig. 8. Transported K<sup>+</sup> beam current as a function of time derived from summing the detector slit data. The total HCX beam current pulse as measured by a Faraday cup is flat; the peaks at the head and tail of the detector signal may be related to variations in beam size at the head and tail of the pulse.

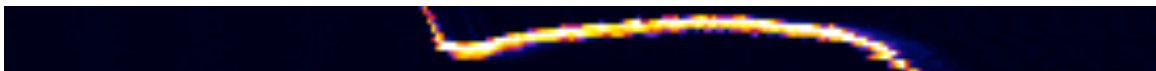


Fig. 9a. Intensity plot of K<sup>+</sup> ion signal during the beam pulse as a function of time. The vertical size of this image is 12.6 keV in beam energy.

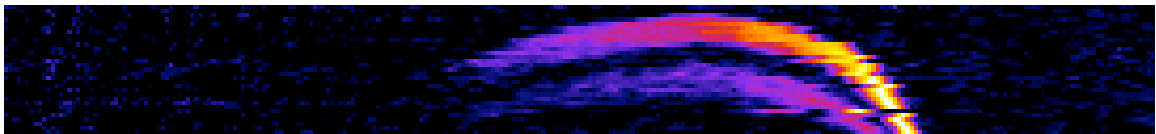


Fig. 9b. Intensity plot of K<sup>++</sup> ion signal during the beam pulse. The hole plate is biased to +9.4 kV. Note the two curves indicating ions from the hole plate (upper curve) and from the entrance slit (lower curve) are cut off before the end of the beam pulse because the analyzer voltage scan ends at that point. The vertical size of this image is 25.2 keV in beam energy.

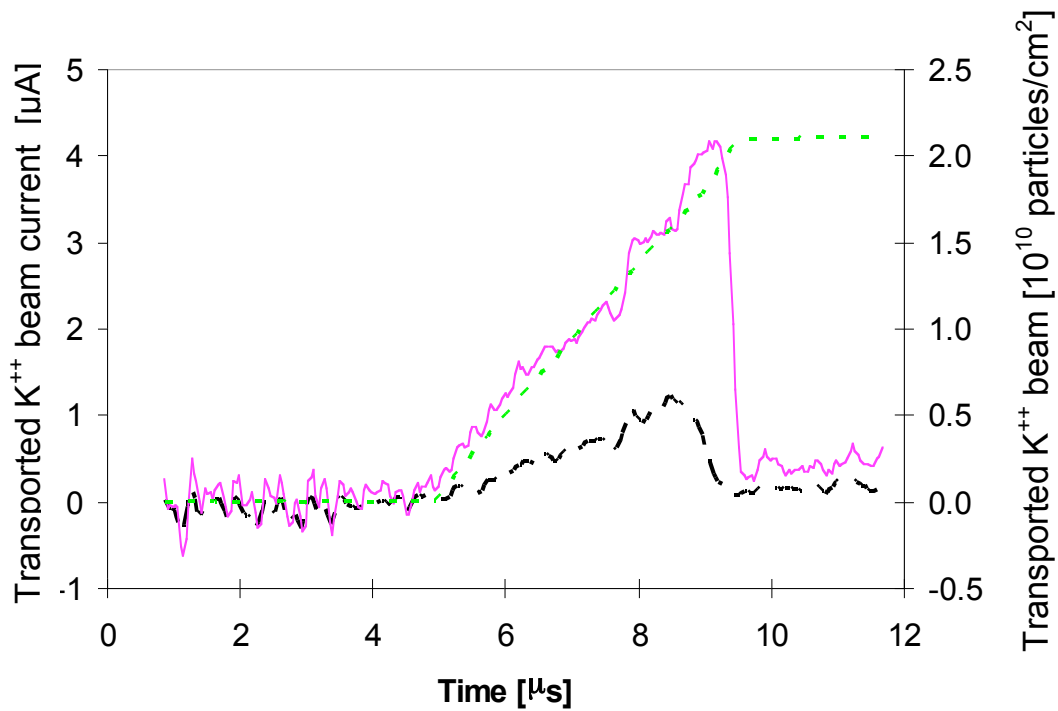


Fig. 10. This is the total  $K^{++}$  ion current (solid magenta),  $K^{++}$  current from the entrance slit only (long dashed black), and the integrated number of transported  $K^+$  ions in the analyzer (short dashed green).

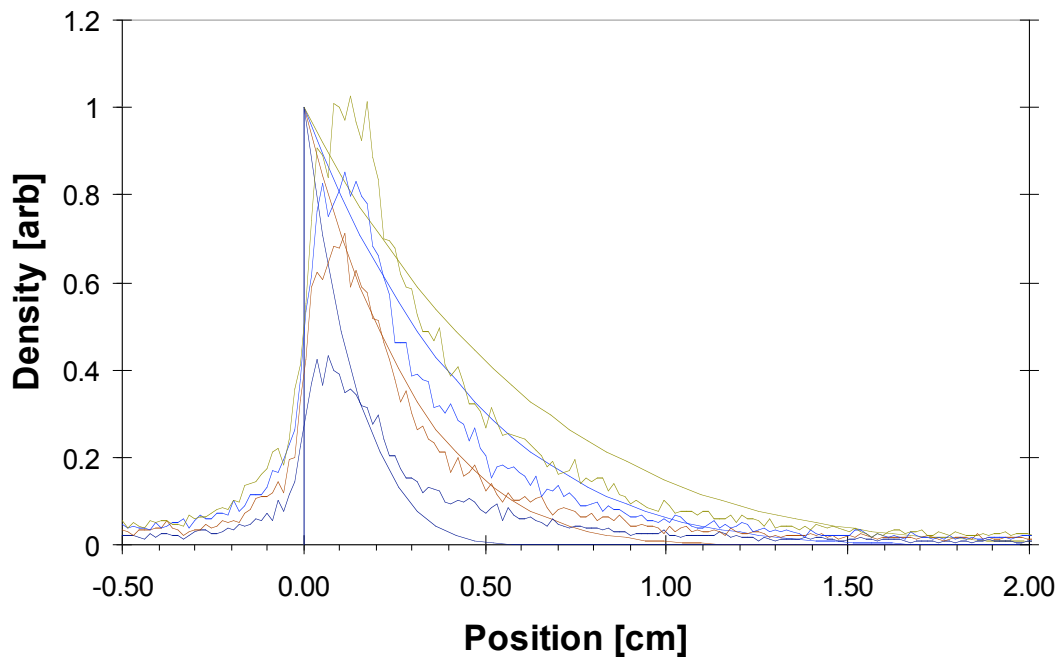


Fig. 11. Experimental profile of light intensity of gas cloud at  $1 \mu\text{s}$  intervals during the beam pulse; density profile from 1-D gas cloud model for  $\text{H}_2$  gas at  $20^\circ\text{C}$ . The smooth curves represent the model profiles.